Computer Modeling in Engineering & Sciences

Tech Science Press

https://doi.org/10.32604/cmes.2026.079804

ARTICLE

Optimising Reinforcement Layout for Enhanced Blast Resistance in RC Slabs: A Numerical Study

Angel Prado[1,*], Alejandro Alañón[2], Ricardo Castedo[3], Anastasio Pedro Santos[3], Lina María López[3] and María Chiquito[3]

[1]Institute of Thermomechanics, Czech Academy of Sciences, Dolejškova 1402/5, Praha, Czech Republic
[2]Escuela Politécnica Superior de Ávila, Universidad de Salamanca, Ávila, Spain
[3]E.T.S.I. Minas y Energía, Universidad Politécnica de Madrid, Madrid, Spain

*Corresponding Author: Angel Prado. Email: prado@it.cas.cz

Received: 28 January 2026; Accepted: 30 March 2026; Published: 27 May 2026

ABSTRACT: This study presents a numerical investigation into the influence of reinforcement layout on the blast response of a reinforced concrete (RC) slab subjected to a close-in explosion. The reference scenario is based on a blast test from the SEGTRANS project using a 15 kg TNT equivalent charge. A validated LS-DYNA model was used, applying the Load Blast Enhanced method and the Continuous Surface Cap Model for concrete behaviour. Forty-nine reinforcement configurations were assessed, all with constant steel mass but varying numbers of longitudinal bars and stirrups. Damage metrics such as eroded elements and internal energy absorption were used to identify an optimal layout consisting of 12 longitudinal bars and 40 stirrups, which reduced the damage volume by 5.72% compared to the original configuration (10 longitudinal bars and 29 stirrups). A further parametric study explored steel mass variations of ±10% and ±20%, applied to bars, stirrups, or both. Twelve additional models confirmed that stirrup reinforcement has a greater influence than longitudinal reinforcement in this slab configuration. To evaluate the robustness of the optimal configuration, 15 more simulations were conducted at scaled distances within the "Near field" range (0.053–0.4 m/kg$^{1/3}$), from 3 to 50 kg. These scenarios, representative of improvised explosive devices, showed a consistent reduction in damage with the optimised layout at the mid- to upper end of the scaled-distance range, but offered no improvement at its lower end due to the near-total structural disintegration of the slab.

KEYWORDS: Blast loading; reinforced concrete; structural optimization; numerical simulation

1 Introduction

The protection of infrastructure against extreme loading conditions such as explosions has gained increasing importance in recent decades, due to the rising prevalence of both accidental and intentional threats. Reinforced concrete (RC) is the most widely used construction material in the world due to its excellent compressive strength, durability, and versatility, as well as its relatively low cost and ease of manufacture. Its ability to be shaped into complex forms and combined with steel reinforcement to resist tensile stresses makes it ideal for a broad range of civil, industrial, and military applications.

RC structures are critical in civil and military infrastructure, and their behaviour under blast loading has been the subject of numerous experimental and numerical investigations [1–3]. The response of such elements depends on various factors, including geometry, explosive energy, stand-off distance, and the internal reinforcement, among others. Given its widespread use, numerous studies have focused on

enhancing the blast resistance of RC structures, either by improving the material properties of concrete itself or by incorporating additional protective layers or strengthening techniques. In terms of intrinsic material enhancement, several studies have focused on improving the properties of concrete to increase its blast resistance. Advances such as high-performance concrete (HPC) and ultra-high-performance concrete (UHPC) have led to higher strength, greater ductility, and improved energy absorption. Recent works such as Fan et al. [4], Xu et al. [5] or Zhang et al. [6] have demonstrated that optimised mix designs, refined aggregate grading, low water-to-cement ratios, and advanced curing methods can significantly enhance the performance of RC elements under blast loading by reducing spalling, delaying crack propagation, and maintaining structural integrity.

In addition to intrinsic material enhancements, the implementation of supplementary protective systems has become a prevalent strategy to further bolster the blast resistance of reinforced concrete (RC) structures. Coatings such as polyurea have demonstrated exceptional performance in mitigating blast-induced damage. For instance, polyurea coatings applied to the surfaces of RC structures have been shown to significantly reduce spalling and enhance energy absorption, thereby improving overall structural integrity under explosive loading [1,7,8]. Similarly, the application of steel plates as external reinforcements has been extensively studied. Research indicates that steel plate retrofitting can effectively increase the load-bearing capacity and ductility of RC elements subjected to blast loads, offering a robust protective measure against explosive impacts [9,10]. Furthermore, the use of fibre-reinforced polymer (FRP) composites, including carbon, glass, and aramid fibres, has been explored to enhance the blast resistance of RC structures [11]. These materials, when applied as wraps or laminates, contribute to increased strength, stiffness, and energy dissipation, thereby improving the structural response to explosive events. Collectively, these supplementary systems, when integrated with high-performance concrete, provide a comprehensive approach to fortifying RC structures against explosive hazards.

The combined use of experimental testing and numerical simulation is the most widespread methodology for investigating the response of RC structures under blast loads [12–14]. Physical experiments, although essential for understanding damage mechanisms and validating models, are often limited by cost, logistical complexity, and safety considerations. For this reason, trials are frequently conducted at reduced scales, with the results extrapolated to real scenarios using appropriate similarity laws [15]. Nevertheless, such extrapolations must be made carefully, as some phenomena (e.g., spalling or localised failure) may not scale linearly [16]. Once validated against experimental data, numerical models enable researchers to simulate a wide range of conditions at a fraction of the cost and time, allowing for parametric studies and predictive analysis. Recent works have increasingly incorporated advanced computational techniques such as artificial intelligence or evolutionary algorithms to improve model calibration and scenario optimisation [17,18].

A variety of commercial software platforms are employed in blast simulations, with LS-DYNA [19] and ANSYS/AUTODYN [20] being among the most widely used. These tools offer multiple modelling strategies for representing both the explosive and the target. The most common blast loading approach is the Load Blast Enhanced (LBE) method, a numerical technique based on experimental TNT blast data [21,22]. However, there exists a wide range of methodologies, among which the most prominent are the Multi-Material Arbitrary Lagrangian-Eulerian (MM-ALE) method [23]; LBE-ALE, a hybrid technique combining LBE and ALE approaches [24]; the Particle Blast Method (PBM) [25]; and Smoothed Particle Hydrodynamics (SPH) [26]. Each of these methods presents its own advantages and disadvantages, such as computational time, ability to adapt to complex geometries, numerical stability, and accuracy in capturing fluid-structure interactions.

Several papers have highlighted the undeniable role of steel reinforcement in improving the structural response against explosions [27,28]. In addition to conventional reinforcement layouts, recent studies

have investigated the use of high-strength rebar and ultra-high-performance concrete (UHPC), reporting enhanced blast resistance under contact and close-in detonations [29,30]. Experimental evidence indicates reduced damage levels, mitigation of penetration, and improved overall structural response compared to conventional reinforcement systems. Previous experimental and numerical investigations have shown that RC slabs subjected to blast loading may experience a transition in failure mode depending on standoff distance and pressure distribution [31]. Near-field detonations tend to promote shear-dominated or localized failure mechanisms, whereas far-field explosions more commonly result in flexural-dominated behaviour. The distribution and intensity of blast pressure have been identified as key parameters governing this transition. Consequently, the relative contribution of longitudinal and transverse reinforcement may vary significantly with scaled distance, particularly under close-in blast conditions. However, most studies related to reinforced concrete under blast loading do not explore different reinforcement configurations, such as varying bar thicknesses or spacing. Instead, they typically follow the recommendations provided by the structural codes of the respective country. Recent investigations have nonetheless demonstrated that the internal architecture and topology of reinforcement can significantly influence blast performance. Innovative solutions such as triply periodic minimal surface scaffolds and 3D-printed Bouligand-inspired concrete panels have shown substantial reductions in damage and deflection through optimisation of reinforcement geometry and fibre alignment. These findings underline the importance of reinforcement layout in governing the dynamic response of concrete elements subjected to explosive loading [32,33].

In this context, the present study employs numerical simulations using LS-DYNA to investigate the influence of various reinforcement configurations on the structural response of RC slabs subjected to close-in detonations. The base model was calibrated in a previous work [34] against full-scale experimental tests conducted on reinforced concrete slabs, providing a reliable initial reference. Among the different slabs tested experimentally, only the one subjected to the highest explosive charge and at a closest standoff distance is considered, as it exhibited the most evident and discernible damage, making it particularly suitable for a meaningful parametric analysis. By systematically varying the reinforcement layout while keeping the total steel mass constant, the study provides insights into how design choices can optimise slab performance under extreme blast loading, potentially informing safer and more cost-effective reinforcement strategies for critical structures.

From this experimentally validated baseline, numerical modifications are introduced to systematically assess the impact of key reinforcement variables. The variables studied include the spacing between both longitudinal bars and stirrups (i.e., transverse reinforcement hoops), which varies according to their total number, the total steel mass involved in the slab and the damage reduction at different scaled distances. This parametric approach eliminates the need for multiple full-scale blast experiments, thereby substantially reducing the economic and logistical cost associated with experimental testing while enabling a broader and controlled research of structural configurations. The results enable the identification of optimal reinforcement layouts that significantly improve blast performance, contributing to the design of safer and more efficient structural solutions.

2 Test Description

The experimental test used in this study was conducted at the Technological Institute “La Marañosa” (Spain) under varying combinations of explosive mass and standoff distance, as part of the SEGTRANS project. This test serves as the basis for the numerical and reference model in the present work.

The test specimen consisted of a reinforced concrete slab with dimensions 4400 mm × 1460 mm × 150 mm, bolted at both ends to concrete blocks, leaving 4 m of the slab exposed from the edge of the supports (see Fig. 1). The reinforced meshing was constructed with 12 mm diameter rebars spaced 150 mm

in both directions, providing a concrete cover of approximately 30 mm on both faces. No additional shear reinforcement was considered necessary.

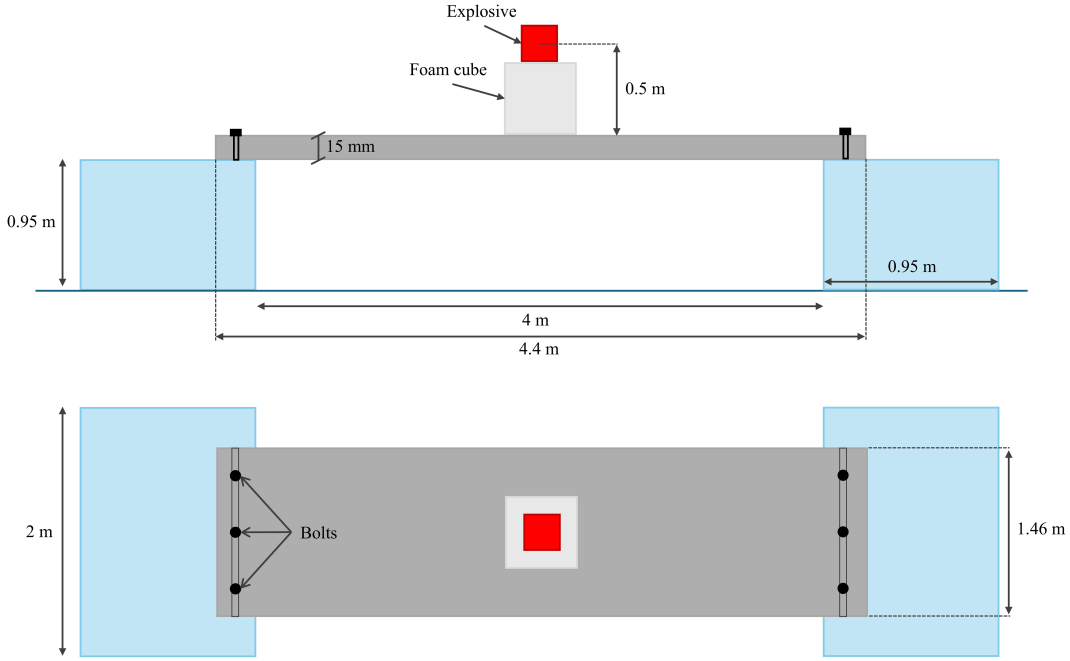

Figure 1: Scheme of the experimental setup.

The explosive employed was PG2, a plastic explosive composed primarily of RDX (86%) with added plasticizers, chosen for its chemical safety, moldability, and well-characterized TNT equivalence on impulse (0.86) as reported by López et al. [35]. An explosive charge of 15 kg TNT-equivalent was used in the present study, cast into cubic shape and elevated 0.5 m above the slab centre using a foam cube, which is assumed to have negligible influence on shock wave propagation [36]. The corresponding scaled distance for the test was 0.20 m/kg$^{1/3}$. No instrumentation was employed during this test to avoid potential damage; therefore, the assessment of the slab response was carried out through post-test measurements, such as the evaluation of crack patterns, fragment displacement, and overall damage. Pre- and post-detonation photographs of the specimen are presented in Fig. 2.

3 Numerical Model Development

Numerical simulations were performed using the explicit finite element code LS-DYNA (Version R13.0), which is particularly well suited for highly nonlinear transient dynamic analyses involving large deformations and blast loading scenarios. The explicit time integration scheme allows stable and efficient computation of short-duration dynamic events without the need for iterative equilibrium procedures at each time step.

The structural elements were discretized using a three-dimensional Lagrangian formulation. The reference configuration corresponds to full-scale slabs; however, to optimize computational cost while preserving the structural response, geometric symmetry was exploited. Therefore, only half of each slab was modelled along its longitudinal axis of symmetry, with appropriate boundary conditions applied at the symmetry plane. The numerical model incorporates detailed representation of the reinforcement layout as well as the corresponding support conditions, as illustrated in Fig. 3. For additional information regarding material models, calibration procedures, and validation, the reader is referred to Castedo et al. [34].

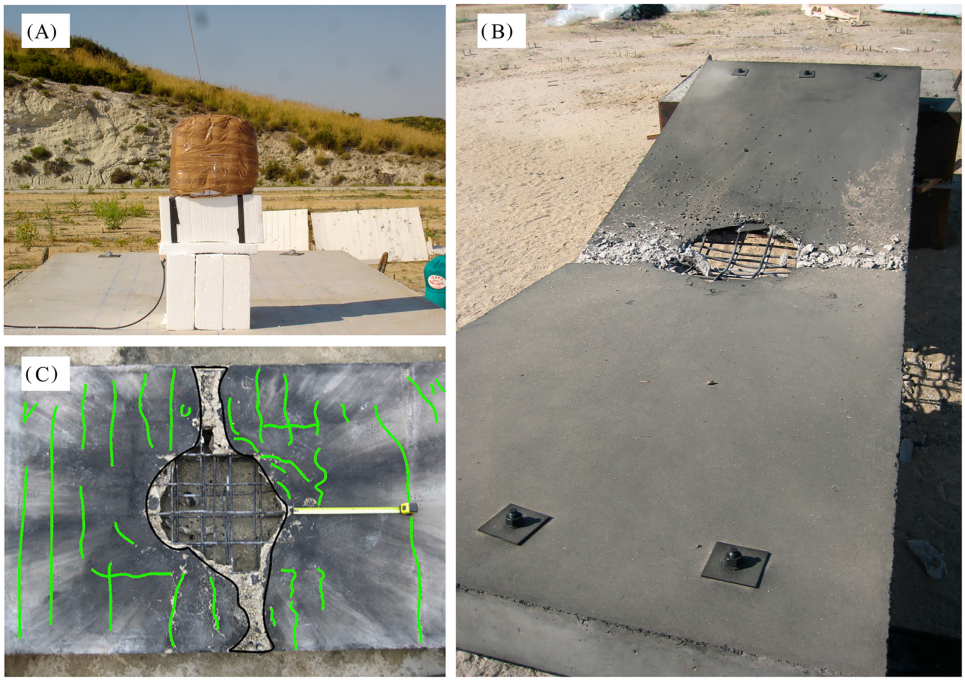

Figure 2: Test photos: (**A**) before detonation; (**B**) and (**C**) after detonation.

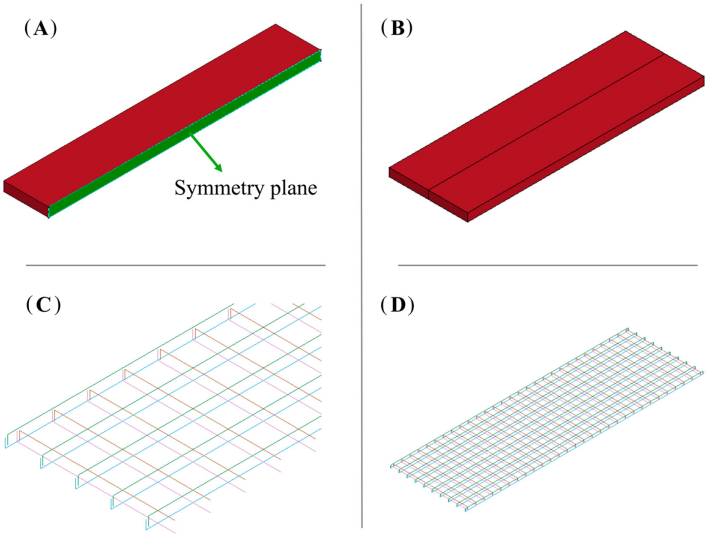

Figure 3: Concrete model showing half (**A**) and full (**B**) views, alongside detailed (**C**) and complete (**D**) reinforcement structures.

The explosive load was modelled using the LBE method, an empirically based approach implemented in LS-DYNA. This technique is based on the ConWep database [37], which comprises pressure–time curves and impulse values derived from a large body of empirical blast tests conducted by the United States Army [38]. These data are formulated through scaled-distance relationships and are used to estimate the peak reflected pressure, arrival time, impulse, and decay of the positive phase generated by a given explosive charge at a specified stand-off distance.

In the present study, the computed pressure–time history is applied directly to the exposed surface of the slab without explicitly modelling the surrounding air domain. The load distribution over the slab surface depends on the discretisation of the target mesh, whereas the global impulse and peak pressure are governed by the explosive charge characteristics and scaled distance. Since the same explosive mass, geometry, stand-off distance, and surface mesh are maintained for all models, the applied blast loading remains consistent throughout the parametric study. It should be noted that the LBE approach reproduces the primary positive phase of the blast wave and does not explicitly account for detailed fluid–structure interaction effects, air confinement, or complex wave reflections. Nevertheless, for the scaled distances considered in this investigation, the method provides a computationally efficient and widely accepted representation of blast loading for structural response analyses.

Concrete was discretized with 3D Lagrangian solid elements and modelled using the Continuous Surface Cap Model (CSCM) material model, while the steel reinforcement was reproduced according to the field test configuration and modelled using the Piecewise Linear Plasticity material model and using beam elements, assuming a perfect bond, i.e., no sliding. This assumption is justified because the loading event is extremely short and characterized by very high blast pressures, leading to strain rates at which bond–slip effects are negligible compared to the overall dynamic response of the slab [39,40]. CSCM material model combines pressure-dependent plasticity with a coupled progressive damage formulation. The model requires as primary input the unconfined compressive strength f_c, from which the remaining constitutive parameters are internally generated through calibration algorithms implemented in the code. This approach allows a mechanically consistent representation of concrete behaviour even when a complete experimental characterization is not available. The constitutive response is defined by multiple pressure-sensitive shear failure surfaces representing the elastic limit, peak strength, and residual strength domains. These surfaces evolve with plastic straining and confinement, enabling the model to reproduce stiffness degradation, strength softening, and compaction effects under high-pressure states typical of blast loading.

Damage evolution is governed by an internal scalar variable d, ranging from 0 (undamaged material) to 1 (fully degraded material). Damage initiates upon reaching the shear plasticity surface and progressively accumulates with increasing inelastic deformation. The term $(1 - d)$ acts as an isotropic degradation factor applied to both bulk and shear moduli, leading to gradual stiffness reduction as damage develops. This coupling between plasticity and stiffness degradation is fundamental for capturing cracking, crushing, and post-peak softening mechanisms. Element erosion is introduced to simulate severe material degradation and fragmentation under extreme loading. When the damage parameter exceeds 0.99 and the maximum principal strain in the element surpasses the user-defined failure threshold (ERODE), the element is removed from the computation. In this work, the conventional ERODE value of 1.05 has been used [41]. The concrete domain was discretised using solid finite elements with a uniform mesh size of 15 mm × 15 mm × 15 mm. The material properties for both concrete and steel are summarised in Table 1.

The validation of the baseline numerical model, whose parameters were selected based on the experimental campaign reported in [34], to ensure realistic material and boundary behaviour, was carried out against full-scale blast-loaded slab tests. The comparison was performed at both global and local response levels. At the global level, the numerical model reproduced the overall structural response, including maximum deflections and the general deformation mode observed experimentally. At the local level, particular attention was given to damage patterns and failure mechanisms. The simulations successfully captured the spatial distribution of cracking and spalling areas, as well as the characteristic localization of damage near the central region of the slab. Quantitatively, the predicted damaged surface areas were compared with post-test measurements, showing discrepancies below 10%. In addition, the model reproduced the main observed failure features, including concrete crushing and localized spalling at the rear face. Based on this combined

qualitative and quantitative agreement, the model is considered to provide a reliable representation of the structural response and damage evolution of the tested slab and therefore serves as a validated baseline for the present study.

Table 1: Constitutive properties of concrete and reinforcing steel.

Property	Concrete	Steel
Density (kg/m^3)	2300	7850
Compressive strength of concrete, f_c (MPa)	25	–
Tensile strength (MPa)	3.7	550.0
Young modulus (MPa)	273×10^2	200×10^3
Yield strength (MPa)	–	500
Tangent modulus (MPa)	–	425

4 Steel Reinforcement Configurations

Building upon the baseline model described in the previous chapter, this study explores the influence of various reinforcement configurations on the damage observed in the RC slab. The original slab featured ten longitudinal bars and twenty-nine stirrups, both with a diameter of Ø12 mm and a concrete cover of 50 mm. Longitudinal bars and stirrups were spaced 15 cm. To investigate the structural response under different configurations, a series of reinforcement layouts was developed by varying the number of longitudinal bars and stirrups while keeping the total steel mass constant. Consequently, the diameters of the reinforcement bars were adjusted accordingly. Although the resulting diameters include decimal values and do not correspond to standard industry sizes, they are employed here to serve the scientific purpose of assessing damage sensitivity to reinforcement distribution.

A total of 49 numerical models were developed, including the baseline model used as a reference. The number of longitudinal bars and the number of stirrups were varied independently, while keeping the total steel mass constant, in order to cover a wide range of configurations (from approximately half to twice the number of bars and stirrups of the original design). All combinations of the values listed below were generated, resulting in $7 \times 7 = 49$ configurations:

- Longitudinal bars: 4, 6, 8, 10, 12, 16, 20
- Stirrups: 15, 20, 25, 29, 40, 50, 60

Fig. 4 shows representative reinforcement layouts, including the original design.

In a second stage of the analysis, the numerical model that exhibited the best performance among the initial 49 configurations is selected as the reference. Based on this optimal reinforcement arrangement, a further parametric study is conducted by varying the total amount of steel by ±10% and ±20%. These changes in steel quantity are applied in three different ways: exclusively to the longitudinal bars, exclusively to the stirrups, and proportionally to both. This analysis adds 12 additional models, and aims to determine whether, in the event of needing to adjust the total steel content, it is more effective to do so by modifying the longitudinal reinforcement, the transverse reinforcement, or both. Lastly, 15 additional simulations were conducted to evaluate the optimal reinforcement design under different scaled distances, bringing the total number of simulations to 76.

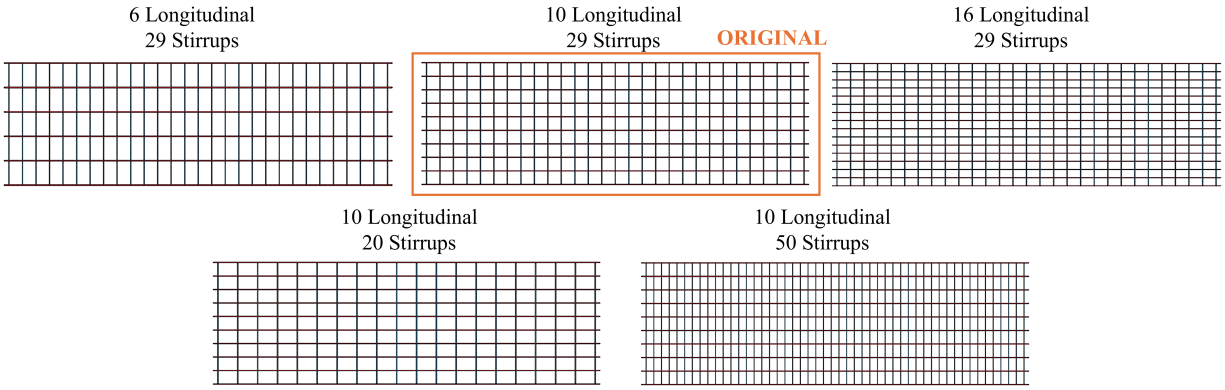

Figure 4: Overview of reinforcement layouts, including the baseline design.

5 Results

This section first presents the results for the optimal configurations of longitudinal bars and stirrups. The number of longitudinal bars and stirrups in the slab was varied, calculating the corresponding bar diameters (which are not market-standard) to maintain the same total steel mass and allow valid comparisons. Next, within the optimal rebar layout identified in the first analysis, the steel mass was modified to assess its influence. Finally, the optimal reinforcement layout was evaluated at different scaled distances.

5.1 Optimal Reinforcement Configuration

To evaluate the improvement or deterioration in the structural response of the RC slab, the number of concrete elements reaching failure (commonly referred to as eroded elements in numerical simulations) is used as a metric. Additionally, the energy absorbed by the slab and graphical outputs from the numerical simulations are employed to support the selection of the optimal numerical model. Each configuration is compared against the baseline model, which exhibited 28,389 eroded elements, corresponding to 95,813 cm^3 of concrete, or 9.94% of the slab's total volume.

Fig. 5 graphically presents the damage sustained by the slab for all models with the same total steel mass. Damage is represented by the number of eroded elements.

Several trends can be identified from the analysis of Fig. 5. It should be noted that the number of eroded elements is influenced not only by the structural configuration but also by factors such as the mesh size, blast modelling technique, and material characteristics. For the present study, however, the baseline model described in Section 3, with a fixed set of parameters validated against experimental data, has been adopted. This approach allows the effects of the steel reinforcement configuration to be assessed independently of other modelling variables.

First, the models incorporating only four longitudinal bars exhibit significantly higher levels of damage compared to the rest, regardless of whether such a configuration might be structurally viable under standard loading conditions. As the number of longitudinal bars increases, the extent of damage in the slab tends to decrease. The models with the highest number of longitudinal bars yield substantially better results when 15, 20, or 25 stirrups are used. However, beyond this range, performance tends to stabilise, although slight improvements are still observed across most configurations. When using 29 stirrups (the original slab configuration), the models with between 10 and 20 longitudinal bars converge towards very similar levels of damage. This suggests that the number of longitudinal bars chosen for the original design was appropriate, as it performs comparably to equivalent models with 12, 16, or even 20 bars. The number of stirrups also has a

significant influence on the structural response. A notable reduction in damage is observed when increasing the stirrup count from 15 to 25. This effect stabilises between 25 and 29 (the baseline model), followed by a further improvement between 29 and 40 stirrups. Beyond 40, performance continues to improve, though at a slower rate, up to 60 stirrups.

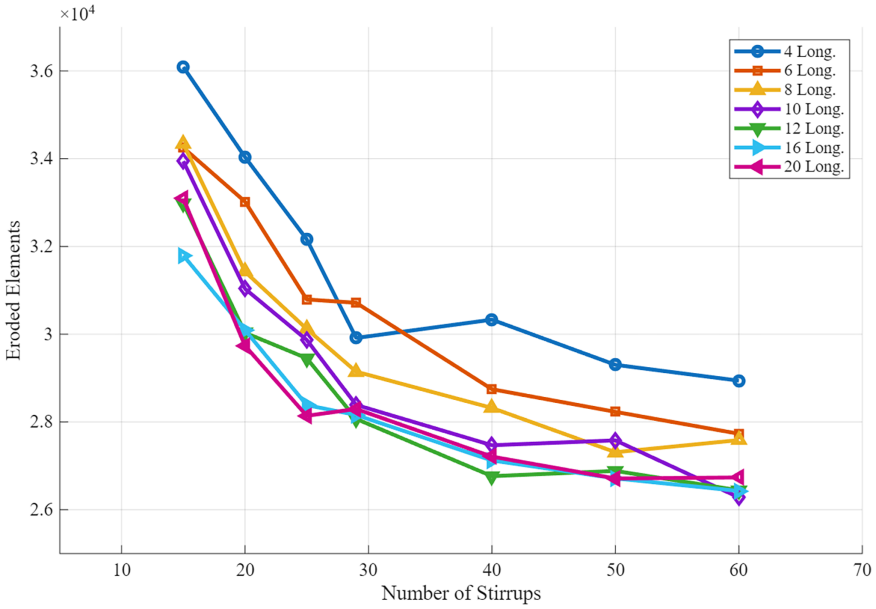

Figure 5: Number of eroded elements in models with varying the number of longitudinal bars ('Long.' in the legend) and stirrups.

The configuration that results in the lowest number of eroded elements corresponds to the model with 10 longitudinal bars and 60 stirrups. However, the models with the same number of stirrups and 16 or 20 longitudinal bars achieve very similar performance. The optimal model achieves a damage reduction of 7.43%. Nonetheless, while the cost of steel is typically proportional to its mass, labour costs must also be considered, as greater assembly time would be required for more complex configurations. For this reason, simpler and more practical configurations are also evaluated.

Among these, the model with 12 longitudinal bars and 40 stirrups stands out. This configuration achieves a 5.72% reduction in damage compared to the original design, which is primarily reflected in a notable reduction of the central perforation visible in Fig. 6. The same steel mass is redistributed across a slightly lower total number of bars (52 vs. 70 in the most effective model), leading to a more efficient reinforcement layout. For this reason, the configuration with 12 longitudinal bars (Ø11 mm spaced 12 cm), and 40 stirrups (Ø10 mm spaced 11 cm) is considered optimal, as it offers an effective balance between structural performance, ease of assembly, and cost. Post-simulation visualisations for these two models are presented in Fig. 6.

Additionally, a graph showing the evolution of the internal energy of the slab (including both concrete and steel) is presented in Fig. 7. The internal energy is used as a key indicator of the structural response under explosive loading, as it represents the portion of the input energy that is absorbed by the slab, providing a quantitative measure of how much energy the structure dissipates during the simulation, making it a useful metric to compare different reinforcement configurations. The top row of Fig. 7 displays the internal energy–time curves for the models with 10 longitudinal bars and varying numbers of stirrups, while the

bottom row shows the results for models with 29 stirrups (original configuration) and varying numbers of longitudinal bars.

A comparison between the plots in both rows of Fig. 7 reveals that variations in the number of stirrups have a greater impact on the internal energy absorbed by the slab than variations in the number of longitudinal bars. This effect is particularly evident in the final stages of the simulation, where fixing the number of longitudinal bars at 10 and varying the stirrups results in larger differences in internal energy between models. In contrast, when the number of stirrups is fixed at 29 (the original configuration), the differences in internal energy between models with varying numbers of longitudinal bars are significantly smaller and less consistent.

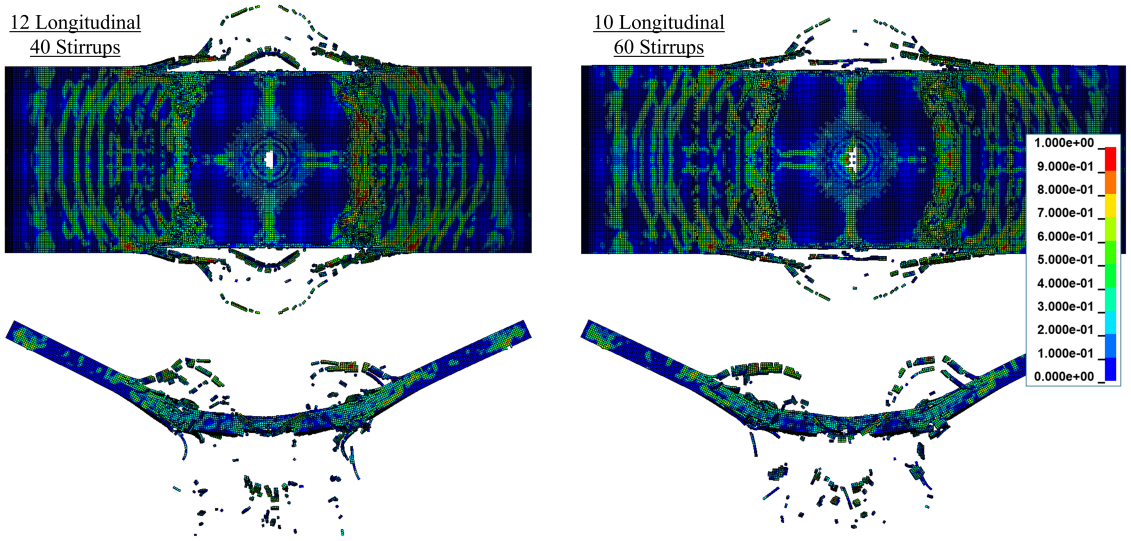

Figure 6: Top and lateral view (first and second row, respectively) of the simulation for the best reinforcement configurations. Legend shows damage (effective plastic strain in CSCM model).

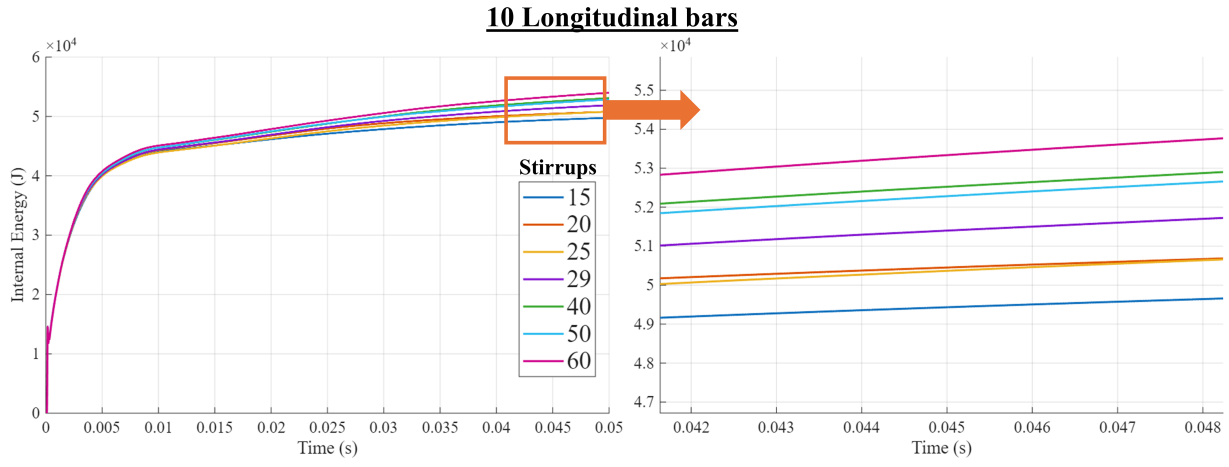

Figure 7: (Continued)

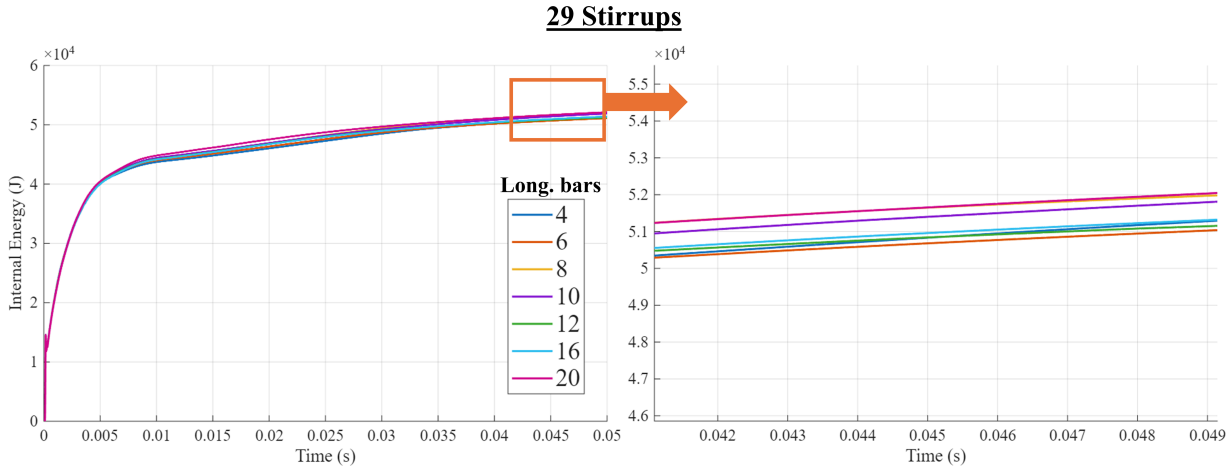

Figure 7: Internal energy–time graphs for the variations in stirrups based on the original longitudinal bar configuration (top row), and for the variations in longitudinal bars based on the original stirrup configuration (bottom row).

Lastly, a comparative study of the beam deflection (vertical displacement at its centre) is presented in Fig. 8. Overall, no significant variations in vertical displacement are observed among the evaluated models. This behaviour is attributed to the high explosive charge applied at a short distance, which causes the slab to reach its maximum displacement prior to failure. Minor variations, however, can be noted: when the number of longitudinal bars is fixed at 10, the maximum displacement slightly increases with a higher number of stirrups, indicating that slabs with these configurations can bend more while retaining more intact elements, as previously discussed in Fig. 5. Similarly, when the number of stirrups is fixed at 29, increasing the number of longitudinal bars allows the slab to reach slightly greater vertical displacements. Nevertheless, as noted earlier, these differences are minimal, suggesting that the number of eroded elements may serve as a more reliable measure for evaluating the effectiveness of the models. It is also important to note that the dynamic characteristics of the slab remain essentially unchanged across the different reinforcement configurations. The numerical results reveal negligible differences in the vibration response, even when comparing the most extreme reinforcement layouts. This behaviour is consistent with the fact that both the peak reflected pressure and the impulse applied to the slab are identical in all simulations, as a consequence of employing the LBE methodology to model the explosive load. Within the LBE approach, the blast loading is governed by the explosive charge mass, geometry, stand-off distance, and the mesh size of the exposed target surface (in this case, the top surface of the slab). Since these parameters, as well as the explosive modelling methodology itself, remain constant across all models, the resulting peak pressure and impulse are likewise unchanged. Consequently, the global dynamic response is controlled predominantly by the applied loading rather than by the relatively modest variations in reinforcement layout, which explains the limited differences observed in the vibration behaviour.

5.2 Influence of Steel Mass on Reinforcement Performance

Based on the findings from the previous section, the configuration with 12 longitudinal bars and 40 stirrups was identified as optimal, offering a balance between damage reduction and ease and cost of construction. Building upon this model, adjustments were made to the total amount of steel used in the slab, introducing four additional variations: −20%, −10%, +10%, and +20% relative to the total steel mass.

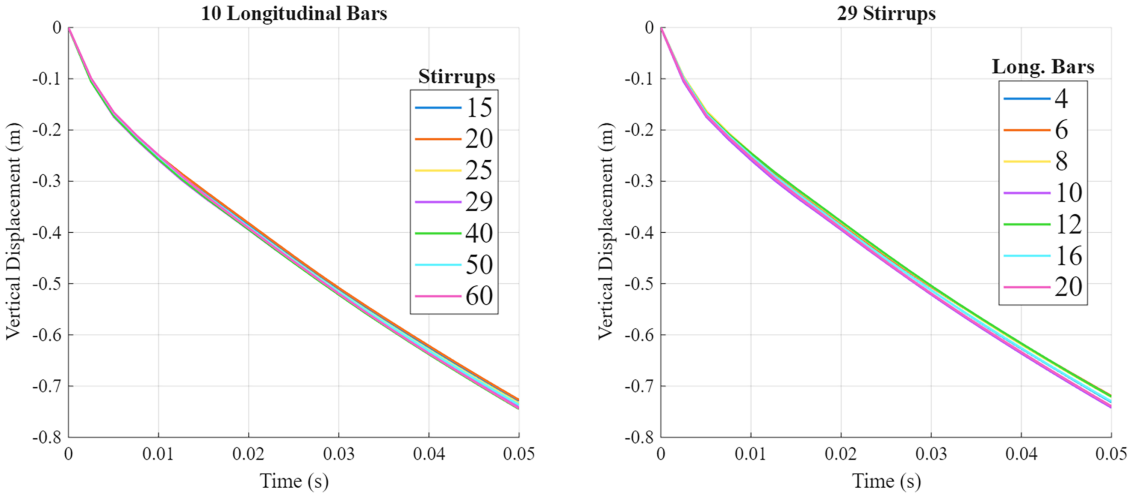

Figure 8: Vertical displacement in time for models with all reinforcement configurations for 10 longitudinal bars (left) and 29 stirrups (right).

To implement these changes, three different approaches were considered:

1. Modifying only the longitudinal bars.
2. Modifying only the stirrups.
3. Modifying both longitudinal bars and stirrups proportionally.

These combinations, along with the base model, are summarised in Table 2, which also includes the number of eroded elements registered in each case.

Table 2: Impact of steel mass distribution adjustments on slab performance.

Total Steel Mass (kg)	Longitudinal Bars Mass (kg)	Stirrups Mass (kg)	Eroded Elements	Relative Difference from the Base Model (%)
150.7	77.6	73.1	28,389	–
120.6	47.5	73.1	30,507	7.46
	77.6	43.0	32,445	14.29
	62.1	58.5	29,936	5.45
135.6	62.5	73.1	28,625	0.83
	77.6	58.0	29,607	4.29
	69.8	65.8	28,624	0.83
165.8	92.7	73.1	26,514	−6.60
	77.6	88.2	25,442	−10.38
	85.4	80.4	26,155	−7.87
180.9	107.8	73.1	24,986	−11.99
	77.6	103.2	24,514	−13.65
	93.1	87.7	26,497	−6.66

From Table 2, it is noteworthy that using the model with 12 longitudinal bars and 40 stirrups, even after a 10% reduction in total steel mass, produces structural responses to the blast that are very similar to those of the baseline model with the full reinforcement (10 longitudinal bars and 29 stirrups). This outcome is only observed when the mass reduction affects either the longitudinal bars alone or both the bars and stirrups together, with damage increases remaining below 1% in both cases. However, when the mass reduction is applied solely to the stirrups (by decreasing their diameter), the difference in damage exceeds 4%. This suggests that the longitudinal bars play a relatively minor role in the slab's ability to mitigate blast effects.

When increasing the total steel mass, all studied models show improvements in damage reduction. Notably, the most significant gains are achieved when the additional steel is concentrated in the stirrups, resulting in 10.38% and 13.65% reductions in damage for models with total steel masses of 165.8 and 180.9 kg, respectively.

This suggests that enhancing the slab's energy dissipation capacity by 10.38% is feasible with only a 10% increase in total steel mass. However, further increasing the steel content by an additional 10% (20% overall) yields only a marginal improvement of 3.27% compared to the previous case, which may not be considered cost-effective from a construction standpoint.

These results reinforce the greater influence of stirrup diameter on the slab's structural performance under blast loading, as opposed to the diameter of the longitudinal bars. Therefore, in reinforced concrete slab design, efforts to enhance blast resistance should prioritise optimisation of the stirrups to achieve more effective outcomes.

5.3 Influence of Scaled Distance

Finally, the configuration previously identified as optimal (12 longitudinal bars and 40 stirrups) was used to assess its performance under various scaled distances and compared to the original base reinforcement layout (10 longitudinal bars and 29 stirrups). The initial numerical model was calibrated for a scaled distance of 0.2 m/kg$^{1/3}$, which, according to the classification by Castedo et al. [42], adapted from Hilding [43], falls within the "Near field" category. This category covers scaled distances between 0.053 and 0.4 m/kg$^{1/3}$.

Within this interval, 15 additional simulations were performed, decreasing the explosive charge linearly from 50 to 3 kg to cover the scaled distance range 0.053–0.4 m/kg$^{1/3}$. These charge weights are consistent with those commonly associated with improvised explosive devices placed in items such as backpacks or suitcases. For each combination of scaled distance and charge, the corresponding standoff distance was calculated based on the given explosive charge, resulting in values between 20 and 0.77 cm.

For the given range of scaled distances, distinct groups can be established based on the size of the blast-induced hole measured on the top surface of the slab. The corresponding measurements are presented in Table 3, which allows for a three-range classification: (1) 0.053–0.152 m/kg$^{1/3}$, where both the optimal and original layouts result in complete slab failure; (2) 0.177–0.251 m/kg$^{1/3}$, where a central hole is formed but the slab remains partially connected, i.e., it is not completely split into two separate pieces; and (3) 0.276–0.4 m/kg$^{1/3}$, where no hole is produced.

For Group 1 (scaled distances 0.053–0.152 m/kg$^{1/3}$), as presented in Table 3, no significant differences were observed between the base and optimal reinforcement layouts, as in all cases the slab experienced complete failure. In this range, the optimal layout reinforcement could not improve the structural response of the slab due to the high explosive charges involved. As example for the result of the slabs, top view of optimal and base models for three models at different scaled distances in this group are presented in Fig. 9.

Table 3: Blast hole area for original and base reinforcement layout configurations. The hole area is calculated by summing the surface area of top-surface eroded finite elements. *Complete Failure is assigned to cases where the hole spans the full width of the slab, splitting it into two separate pieces.

Group	Scaled Distance (m/kg$^{1/3}$)	Hole Area—Base Model (cm^2)	Hole Area—Optimal Model (cm^2)
1	0.053; 0.078; 0.103; 0.127; and 0.152	Complete Failure*	Complete Failure
2	0.177	Complete Failure	1331
	0.202	746	505
	0.227	40	11
	0.251	4	0
3	0.276; 0.301; 0.326; 0.350; 0.375; and 0.4	0	0

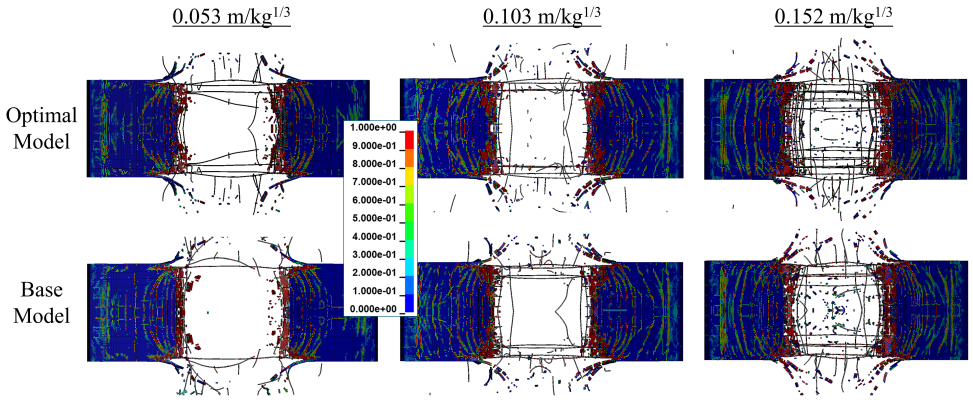

Figure 9: Top view comparison of optimal and base models for Group 1 (according to Table 3).

For Group 2 (scaled distances 0.177–0.251 m/kg$^{1/3}$), the results reveal a consistent trend. The optimal layout reduces the central hole area compared to the base model across the entire range of scaled distances. At 0.177 m/kg$^{1/3}$, the optimal model withstands the blast without splitting into two pieces, whereas the base model undergoes complete failure. At the other end of the range, at 0.251 m/kg$^{1/3}$, the base model still develops a small central hole, while the optimal model shows no central hole formation despite minor damage.

For Group 3 (scaled distances 0.276–0.4 m/kg$^{1/3}$), no hole is produced in either layout, indicating that both configurations are capable of fully resisting the blast at these scaled distances. As magnitude for comparison, the maximum deformation (i.e., as the maximum vertical displacement of the slab from the initial position) for Group 3 models is presented in Table 4. The results show that the differences between the base and optimised layouts are generally small, ranging from −4.8% to 0.5%, indicating that the optimisation provides only minor improvements in maximum displacement. Overall, the optimised layout slightly reduces the maximum displacement in most cases, suggesting a marginal benefit in structural performance.

Table 4: Maximum vertical displacement of slabs for Group 3 (scaled distances 0.276–0.4 m/kg$^{1/3}$) for base and optimised reinforcement layouts.

Scaled Distance (m/kg$^{1/3}$)	Max. Displacement—Base Model (cm)	Max. Displacement—Optimal Model (cm)	Relative Difference (%)
0.276	93.2	90.5	−2.9
0.301	74.7	75.1	0.5
0.326	58.0	57.9	−0.2
0.350	43.4	41.3	−4.8
0.375	30.0	29.4	−2.0
0.400	15.1	14.9	−1.3

6 Conclusions

This study presents a thorough numerical investigation into how the distribution of steel reinforcement affects the blast response of a reinforced concrete (RC) slab subjected to a close-in detonation. Starting from a validated baseline model based on an experimental test from the SEGTRANS project, a parametric study was conducted by systematically varying the number of longitudinal bars and stirrups while keeping the total steel mass constant. Initially, 49 reinforcement configurations were analysed, followed by 12 additional models where the total steel amount was adjusted by ±10% and ±20%, applied to longitudinal bars, stirrups, or both. The study concluded with 15 further simulations to evaluate the influence of scaled distance on the damage mitigation achieved by the optimal configuration. The results showed that:

(1) Longitudinal bars and stirrups effect: Too few longitudinal bars (e.g., 4) drastically increase damage. Increasing bars improves performance, though with diminishing returns, while increasing stirrups from 15 to 40 yields the most notable mitigation; further increases provide smaller gains.
(2) Optimal configuration: Among constant-mass models, 12 longitudinal bars and 40 stirrups achieved a 5.72% damage reduction compared to the original 10-bar, 29-stirrup model, while remaining feasible for construction.
(3) Internal energy analysis: Variations in stirrup number influence structural response more than longitudinal bars, indicating transverse reinforcement is more effective for blast resistance improvements.
(4) Effect of total steel mass: Increasing steel mass (±10% and ±20%) further reduced damage, particularly when added to stirrups (up to 13.65%), but additional increases show limited benefit, confirming cost-effective stirrup optimisation should be prioritised.
(5) Scaled distance effects: Testing across 15 scaled distances (0.053–0.4 m/kg$^{1/3}$, 3–50 kg explosives) showed maximum damage reduction at mid-range distances, marginal improvements at high distances, and negligible effect at very low distances due to complete slab failure.

In conclusion, this study demonstrates that the resistance of RC slab performance under blast loading can be significantly enhanced by optimising reinforcement layout and, where appropriate, increasing the total steel mass. Beyond the immediate numerical findings, these results provide practical insights for structural designers, enabling more effective and economically viable reinforcement strategies. For instance, prioritising stirrup distribution over longitudinal bars may yield greater improvements in blast resistance for a given steel mass, and the parametric trends identified here could inform guidelines for protective design of critical infrastructure, such as military facilities, transport hubs, and industrial plants. However, this study is limited to numerical simulations and has not yet been validated experimentally. Future work could extend

these concepts to multi-span slabs, slabs with openings, or full-scale structures to validate applicability in real-world scenarios.

Acknowledgement: The authors also wish to thank MAXAM Civil Explosives and the Technological Institute "La Marañosa" for their valuable support and collaboration. Also, the authors acknowledge the institutional support RVO:61388998.

Funding Statement: This study makes use of experimental data obtained within the framework of the SEGTRANS project, funded by the Centre for the Development of Industrial Technology (CDTI, Government of Spain).

Author Contributions: The authors confirm contribution to the paper as follows: Conceptualization, Alejandro Alañón; methodology, Angel Prado and Alejandro Alañón; software, Angel Prado and Ricardo Castedo; validation, Angel Prado and Ricardo Castedo; formal analysis, Angel Prado, Alejandro Alañón and Ricardo Castedo; investigation, Ricardo Castedo, Anastasio Pedro Santos, Lina María López and María Chiquito; resources, Ricardo Castedo, Anastasio Pedro Santos, Lina María López and María Chiquito; data curation, Ricardo Castedo, Anastasio Pedro Santos, Lina María López and María Chiquito; writing—original draft preparation, Angel Prado; writing—review and editing, Ricardo Castedo and Anastasio Pedro Santos; visualization, Angel Prado; supervision, Alejandro Alañón and Ricardo Castedo; project administration, Anastasio Pedro Santos and Lina María López; funding acquisition, Anastasio Pedro Santos and Lina María López. All authors reviewed and approved the final version of the manuscript.

Availability of Data and Materials: Data available on request from the authors. The data that support the findings of this study are available from the corresponding author, Angel Prado, upon reasonable request.

Ethics Approval: Not applicable.

Conflicts of Interest: The authors declare no conflicts of interest.

Abbreviations

RC	Reinforced Concrete
TNT	Trinitrotoluene
HPC	High-Performance Concrete
UHPC	Ultra-High-Performance Concrete
FRP	Fibre-Reinforced Polymer
LBE	Load Blast Enhanced
MM-ALE	Multi-Material Arbitrary Lagrangian–Eulerian
ALE	Arbitrary Lagrangian–Eulerian
PBM	Particle Blast Method
SPH	Smoothed Particle Hydrodynamics
ConWep	Conventional Weapons Effects Program
CSCM	Continuous Surface Cap Model

References

1. Yang C, Jia X, Huang Z, Zhao L, Shang W. Damage of full-scale reinforced concrete beams under contact explosion. Int J Impact Eng. 2022;163(1):104180. doi:10.1016/j.ijimpeng.2022.104180.
2. Zhu W, Yang C, Yin T, Jia J, Yu J, Song J. Blast resistant performance and damage mechanism of steel reinforced concrete beams under contact explosion. Eng Struct. 2024;315(5):118472. doi:10.1016/j.engstruct.2024.118472.
3. Liu Z, Jiang N, Zhou C, Ji L, Luo X. Damage effect of terrorist attack explosion-induced shock wave in a double-deck island platform metro station. Period Polytech Civ Eng. 2021;65(1):215–28.

4. Fan Y, Chen L, Yu R, Xiang H, Fang Q. Experimental study of damage to ultra-high performance concrete slabs subjected to partially embedded cylindrical explosive charges. Int J Impact Eng. 2022;168(102):104298. doi:10.1016/j.ijimpeng.2022.104298.
5. Xu Z, Li J, Wu C. A numerical study of blast resistance of fire damaged ultra-high performance concrete columns. Eng Struct. 2023;279:115613. doi:10.1016/j.engstruct.2023.115613.
6. Zhang W, Mao J, Zhou B, Yu X, Hu F, Wang L, et al. The impacts of contact explosions on ultra-high performance reinforced concrete slabs: experimental study and dimensional analysis. Sci Rep. 2024;14(1):25700. doi:10.1038/s41598-024-74774-x.
7. Iqbal N, Sharma PK, Kumar D, Roy PK. Protective polyurea coatings for enhanced blast survivability of concrete. Constr Build Mater. 2018;175(5):682–90. doi:10.1016/j.conbuildmat.2018.04.204.
8. Lyu P, Fang Z, Wang X, Huang W, Zhang R, Sang Y, et al. Explosion test and numerical simulation of coated reinforced concrete slab based on BLAST mitigation polyurea coating performance. Materials. 2022;15(7):2607. doi:10.3390/ma15072607.
9. Thai DK, Pham TH, Nguyen DL. Damage assessment of reinforced concrete columns retrofitted by steel jacket under blast loading. Structural Design Tall Build. 2020;29(1):e1676. doi:10.1002/tal.1676.
10. Chen GQ, Lu JX, Wu H. Dynamic behavior and retrofitting of RC frame building under vehicular bomb explosion. Eng Fail Anal. 2023;143(3):106925. doi:10.1016/j.engfailanal.2022.106925.
11. Hosseini M, Jian B, Zhang J, Li H, Lorenzo R, Hosseini A, et al. Numerical study on the behaviour of hybrid FRPs reinforced RC slabs subjected to blast loads. J Renew Mater. 2023;11(9):3517–31. doi:10.32604/jrm.2023.028164.
12. Yan J, Liu Y, Xu Z, Li Z, Huang F. Experimental and numerical analysis of CFRP strengthened RC columns subjected to close-in blast loading. Int J Impact Eng. 2020;146:103720. doi:10.1016/j.ijimpeng.2020.103720.
13. Prado A, Alañón A, Castedo R, Santos AP, López LM, Chiquito M, et al. Resistance of full-scale beams against close-in explosions. Numerical modeling and field tests. Def Technol. 2024;40(15):35–47. doi:10.1016/j.dt.2024.05.002.
14. Draganić H, Jeleč M, Gazić G, Lukić S. Numerical investigations of reinforced concrete slabs subjected to contact explosions. Buildings. 2025;15(7):1063. doi:10.3390/buildings15071063.
15. Morsel A, Masi F, Kotronis P, Stefanou I. Measurement, self-similarity, and TNT equivalence of blasts from exploding wires. Shock Waves. 2025;35(1):17–35. doi:10.1007/s00193-024-01209-x.
16. Zhao C, Wang Q, Lu X, Huang X, Mo YL. Blast resistance of small-scale RCS in experimental test and numerical analysis. Eng Struct. 2019;199(3):109610. doi:10.1016/j.engstruct.2019.109610.
17. Almustafa MK, Nehdi ML. Machine learning model for predicting structural response of RC columns subjected to blast loading. Int J Impact Eng. 2022;162(4):104145. doi:10.1016/j.ijimpeng.2021.104145.
18. Razavi Tosee SV, Faridmehr I, Nehdi ML, Plevris V, Valerievich KA. Predicting crack width in CFRP-strengthened RC one-way slabs using hybrid grey wolf optimizer neural network model. Buildings. 2022;12(11):1870. doi:10.3390/buildings12111870.
19. ANSYS. LS-DYNA keyword user's manual. Vol. I, II and III—R15. Canonsburg, PA, USA: ANSYS; 2025.
20. ANSYS. ANSYS AUTODYN manual version 2024 R2. Canonsburg, PA, USA: ANSYS; 2024.
21. Zhang C, Abedini M. Time-history blast response and failure mechanism of RC columns using Lagrangian formulation. Structures. 2021;34(4):3087–98. doi:10.1016/j.istruc.2021.09.073.
22. Nawar MT, Elshazli MT, Elzohairy A, Eisa A, Salim H. Improving blast resistance of reinforced concrete beams using recycled rubber integration. Structures Congr. 2025;2025:73–85. doi:10.1061/9780784486085.007.
23. Debnath J, Kumar A, Sharma H. Numerical investigation of reinforced-concrete beam-column joints under contact and close-in blast application. ASPS Conf Proc. 2022;1(1):1203–8. doi:10.38208/acp.v1.641.
24. Kim Y, Lee K, Shin J. Ductility and residual strength-based blast resistance evaluation of RC columns with various structural details. Structures. 2025;77(1):109179. doi:10.1016/j.istruc.2025.109179.
25. Liu J, Zhou Y, Zhang M, Bai J, Xiao W. Analysis of prefabricated fragment intrusion damage based on complete restart technique. In: Proceedings of the 5th International Conference on Advances in Manufacturing and Materials Engineering (ICAMME 2022); 2022 Aug 9–10; Kuala Lumpur, Malaysia. p. 51–62. doi:10.1007/978-981-99-2375-5_6.

26. Cao K, Tang C, Zhao Y, Huang H, Bai W, Zhang L. Evaluation of the performance and effect of steel fiber reinforced cellular concrete for underwater blast protection under contact explosion loading. Eng Fract Mech. 2025;313(29):110668. doi:10.1016/j.engfracmech.2024.110668.
27. Štoller J, Dvořák P. Experimental ballistic loading of steel fiber reinforced concrete slabs and unreinforced concrete slabs by plastic explosives. In: Durability of critical infrastructure, monitoring and testing. Singapore: Springer; 2016. p. 110–9. doi:10.1007/978-981-10-3247-9_13.
28. Dua A, Braimah A. Assessment of reinforced concrete slab response to contact explosion effects. J Perform Constr Facil. 2020;34(4):04020061. doi:10.1061/(asce)cf.1943-5509.0001469.
29. Li J, Wu C, Hao H. An experimental and numerical study of reinforced ultra-high performance concrete slabs under blast loads. Mater Des. 2015;82(12):64–76. doi:10.1016/j.matdes.2015.05.045.
30. Wang J, Xu Y, Wang S, Zhang W, Ji X, Zhang B. Effect of high-strength rebar and ultra-high-performance concrete on blast resistance of slabs under contact explosion loads. Int J Impact Eng. 2025;198:105230. doi:10.1016/j.ijimpeng.2025.105230.
31. Syed ZI, Raman SN, Ngo T, Mendis P, Pham T. The failure behaviour of reinforced concrete panels under far-field and near-field blast effects. Structures. 2018;14(1):220–9. doi:10.1016/j.istruc.2018.03.009.
32. Nguyen-Van V, Peng C, Hazell PJ, Lee J, Nguyen-Xuan H, Tran P. Performance of meta concrete panels subjected to explosive load: numerical investigations. Struct Concr. 2025;26(5):5807–24. doi:10.1002/suco.202200749.
33. Nguyen-Van V, Tran P, Ha NS, Xie YM, Aslani F. Blast resistance of 3D-printed Bouligand concrete panels reinforced with steel fibers: numerical investigations. Compos Struct. 2024;348(8):118481. doi:10.1016/j.compstruct.2024.118481.
34. Castedo R, Segarra P, Alañon A, Lopez LM, Santos AP, Sanchidrian JA. Air blast resistance of full-scale slabs with different compositions: numerical modeling and field validation. Int J Impact Eng. 2015;86(5):145–56. doi:10.1016/j.ijimpeng.2015.08.004.
35. López L, Sanchidrián J, Piedra L, Ríos J. Shock wave pressure in underground explosions. In: Explosives and blasting technique. London, UK: Taylor & Francis; 2003. p. 441–7. doi:10.1201/9781439833476.ch54.
36. Bickes RW, Bonzon LL, inventors. Corporation S, assignee. Explosive scabbling of structural materials. US 6,438,191 B1. 2002 Aug 20.
37. Kingery CN, Bulmash G. Airblast parameters from TNT spherical air burst and hemispherical surface burst. Aberdeen, MD, USA: Ballistic Research Laboratories; 1984.
38. Hyde DW. CONWEP: conventional weapons effects program. Vicksburg, MS, USA: US Army Engineer Waterways Experiment Station; 1991.
39. Liu Y, Hao H, Hao Y. Prediction of blast response of RC columns considering dynamic bond-slip between reinforcement and concrete. Eng Struct. 2023;283:115921. doi:10.1016/j.engstruct.2023.115921.
40. Zhou XQ, Kuznetsov VA, Hao H, Waschl J. Numerical prediction of concrete slab response to blast loading. Int J Impact Eng. 2008;35(10):1186–200. doi:10.1016/j.ijimpeng.2008.01.004.
41. Murray YD, Abu-Odeh A, Bligh RP. Evaluation of LS-DYNA concrete material model 159. McLean, VA, USA: Federal Highway Administration; 2007. Report No.: FHWA-HRT-05-063.
42. Castedo R, Santos AP, Alañón A, Reifarth C, Chiquito M, López LM, et al. Numerical study and experimental tests on full-scale RC slabs under close-in explosions. Eng Struct. 2021;231:111774. doi:10.1016/j.engstruct.2020.111774.
43. Hilding D. Methods for modelling air blast on structures in LS-DYNA. In: Proceedings of the Nordic LS-DYNA Users' Conference; 2016 Oct 13–14; Gothenburg, Sweden.